Behaviour of the Dam-Break Problem for the Serre Equations

Jordan Pitt,[1]
Christopher Zoppou,[1]
Stephen G. Roberts,[1]

ABSTRACT

Keywords: dispersive waves, conservation laws, Serre equation, finite volume method, finite difference method

INTRODUCTION

SERRE EQUATIONS

The Serre equations can derived as an approximation to the full Euler equations by depth integration similar to (Su and Gardner 1969). They can also be seen as an asymptotic expansion to the Euler equations as well (Lannes and Bonneton 2009). The former is more consistent with the perspective from which numerical methods will be developed while the latter indicates the appropriate regions in which to use these equations as a model for fluid flow. The set up of the scenario under which the Serre approximation is made consists of a two dimensional $\mathbf{x} = (x, z)$ fluid over a bottom topography as in Figure 1 acting under gravity. Consider a fluid particle at depth $\xi(\mathbf{x}, t) = z - h(x, t) - z_b(x)$ below the water surface, see Figure 1. Where the water depth is $h(x, t)$ and $z_b(x)$ is the bed elevation. The fluid particle is subject to the pressure, $p(\mathbf{x}, t)$ and gravitational acceleration, $\mathbf{g} = (0, g)^T$ and has a velocity $\mathbf{u} = (u(\mathbf{x}, t), w(\mathbf{x}, t))$, where $u(\mathbf{x}, t)$ is the velocity in the x-coordinate and $w(\mathbf{x}, t)$ is the velocity in the z-coordinate and t is time. Assuming that $z_b(x)$ is constant the Serre equations read (Li et al. 2014)

$$\frac{\partial h}{\partial t} + \frac{\partial (\bar{u} h)}{\partial x} = 0 \tag{1a}$$

[1]Mathematical Sciences Institute, Australian National University, Canberra, ACT 0200, Australia, E-mail: Jordan.Pitt@anu.edu.au. The work undertaken by the first author was supported financially by an Australian National University Scholarship.

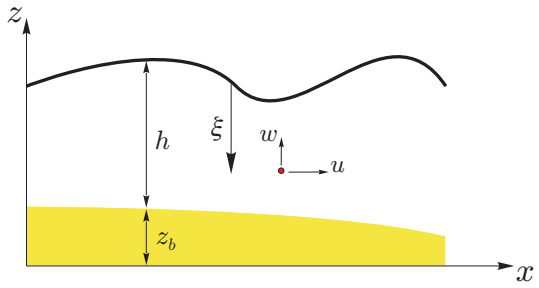

FIG. 1: The notation used for one-dimensional flow governed by the Serre equation.

$$\underbrace{\underbrace{\frac{\partial(\bar{u}h)}{\partial t}+\frac{\partial}{\partial x}\left(\bar{u}^2h+\frac{gh^2}{2}\right)}_{\text{Shallow Water Wave Equations}}+\underbrace{\frac{\partial}{\partial x}\left(\frac{h^3}{3}\left[\frac{\partial\bar{u}}{\partial x}\frac{\partial\bar{u}}{\partial x}-\bar{u}\frac{\partial^2\bar{u}}{\partial x^2}-\frac{\partial^2\bar{u}}{\partial x\partial t}\right]\right)}_{\text{Dispersion Terms}}}_{\text{Serre Equations}}=0. \tag{1b}$$

Where $\bar{u}$ means the average of u over the depth of water.

DIRECT NUMERICAL METHODS

Due to the presence of the mixed spatial and temporal derivatives in the conservation of momentum equation (1b) the choices of methods for these particular equations are limited. Thus the two direct numerical methods presented in this paper will begin by approximating (1b) by finite differences. To facilitate this a uniform grid in space will be used with $\Delta x = x_{i+1} - x_i$ for all i and quantities evaluated at these grid points will be denoted by subscripts for example $h_i = h(x_i)$. The grid in time will be denoted by superscripts for example $h^n = h(t^n)$, noting that h^n is a function in space.

Finite Difference Appximation to Conservation of Momentum Equation

In [][Zoppou thesis/my work] it was demonstrated that an efficient numerical scheme for the Serre equations must be at least second-order accurate thus the derivatives in (1b) will be approximated by second-order finite differences. Firstly (1b) must be expanded, making use of (1a) one obtains

$$h\frac{\partial u}{\partial t}+X-h^2\frac{\partial^2u}{\partial x\partial t}-\frac{h^3}{3}\frac{\partial^3u}{\partial x^2\partial t}=0 \tag{2a}$$

where X contains only spatial derivatives and is

$$X=uh\frac{\partial u}{\partial x}+gh\frac{\partial h}{\partial x}+h^2\frac{\partial u}{\partial x}\frac{\partial u}{\partial x}+\frac{h^3}{3}\frac{\partial u}{\partial x}\frac{\partial^2u}{\partial x^2}-h^2u\frac{\partial^2u}{\partial x^2}-\frac{h^3}{3}u\frac{\partial^3u}{\partial x^3} \tag{2b}$$

where the bar over u has been dropped to simplify notation. Then taking second-order centred finite difference approximation to the time derivatives for (2a) gives

$$h^n \frac{u^{n+1} - u^{n-1}}{2\Delta t} + X^n - (h^n)^2 \frac{\left(\frac{\partial u}{\partial x}\right)^{n+1} - \left(\frac{\partial u}{\partial x}\right)^{n-1}}{2\Delta t} - \frac{(h^n)^3}{3} \frac{\left(\frac{\partial^2 u}{\partial x^2}\right)^{n+1} - \left(\frac{\partial^2 u}{\partial x^2}\right)^{n-1}}{2\Delta t} = 0,$$

$$h^n \left(u^{n+1} - u^{n-1}\right) + 2\Delta t X^n - (h^n)^2 \left(\left(\frac{\partial u}{\partial x}\right)^{n+1} - \left(\frac{\partial u}{\partial x}\right)^{n-1}\right) - \frac{(h^n)^3}{3} \left(\left(\frac{\partial^2 u}{\partial x^2}\right)^{n+1} - \left(\frac{\partial^2 u}{\partial x^2}\right)^{n-1}\right) = 0.$$

Introducing

$$Y^n = 2\Delta t X^n - h^n u^{n-1} + (h^n)^2 \left(\frac{\partial u}{\partial x}\right)^{n-1} + \frac{(h^n)^3}{3} \left(\frac{\partial^2 u}{\partial x^2}\right)^{n-1}$$

and rearranging results in

$$h^n u^{n+1} - (h^n)^2 \left(\frac{\partial u}{\partial x}\right)^{n+1} - \frac{(h^n)^3}{3} \left(\frac{\partial^2 u}{\partial x^2}\right)^{n+1} + Y^n = 0.$$

Taking second-order approximations to the spatial derivatives and evaluating the quantities at the correct locations gives

$$h_i^n u_i^{n+1} - (h_i^n)^2 \left(\frac{u_{i+1}^{n+1} - u_{i-1}^{n+1}}{2\Delta x}\right) - \frac{\left(h_i^n\right)^3}{3} \left(\frac{u_{i+1}^{n+1} - 2u_i^{n+1} + u_{i-1}^{n+1}}{\Delta x^2}\right) = -Y_i^n \tag{3}$$

This can be rearranged into a tri-diagonal matrix that updates u given its current and previous values. So that

$$\begin{bmatrix} u_0^{n+1} \\ \vdots \\ u_m^{n+1} \end{bmatrix} = A^{-1} \begin{bmatrix} -Y_0^n \\ \vdots \\ -Y_m^n \end{bmatrix} =: \mathcal{G}_u \left(\boldsymbol{u}^n, \boldsymbol{h}^n, \boldsymbol{u}^{n-1}, \boldsymbol{h}^{n-1}, \Delta x, \Delta t\right). \tag{4}$$

Where

$$A = \begin{bmatrix} b_0 & c_0 & & & & & \\ a_0 & b_1 & c_1 & & & & \\ & a_1 & b_2 & c_2 & & & \\ & & \ddots & \ddots & \ddots & & \\ & & & a_{m-3} & b_{m-2} & c_{m-2} & \\ & & & & a_{m-2} & b_{m-1} & c_{m-1} \\ & & & & & a_{m-1} & b_m \end{bmatrix}$$

with

$$a_{i-1} = \frac{\left(h_i^n\right)^2}{2\Delta x}\frac{h_{i+1}^n - h_{i-1}^n}{2\Delta x} - \frac{\left(h_i^n\right)^3}{3\Delta x^2}, \tag{5a}$$

$$b_i = h_i^n + \frac{2h_i^n}{3\Delta x^2} \tag{5b}$$

and

$$c_i = -\frac{\left(h_i^n\right)^2}{2\Delta x}\frac{h_{i+1}^n - h_{i-1}^n}{2\Delta x} - \frac{\left(h_i^n\right)^3}{3\Delta x^2}. \tag{5c}$$

Lastly for completeness the final expression for Y_i^n is given by

$$\begin{aligned} Y_i^n = 2\Delta t\Bigg[& u_i^n h_i^n \frac{u_{i+1}^n - u_{i-1}^n}{2\Delta x} + g h_i^n \frac{h_{i+1}^{n-1} - h_{i-1}^{n-1}}{2\Delta x} + \left(h_i^n\right)^2 \left(\frac{u_{i+1}^{n-1} - u_{i-1}^{n-1}}{2\Delta x}\right)^2 \\ & + \frac{\left(h_i^n\right)^3}{3}\frac{u_{i+1}^n - u_{i-1}^n}{2\Delta x}\frac{u_{i+1}^n - 2u_i^n + u_{i-1}^n}{\Delta x^2} - \left(h_i^n\right)^2 u_i^n \frac{u_{i+1}^n - 2u_i^n + u_{i-1}^n}{\Delta x^2} \\ & - \frac{\left(h_i^n\right)^3}{3} u_i^n \frac{u_{j+2}^n - 2u_{j+1}^n + 2u_{j-1}^n - u_{j-2}^n}{2\Delta x^3}\Bigg] \\ & - h_i^n u_i^{n-1} + \left(h_i^n\right)^2 \frac{u_{i+1}^{n-1} - u_{i-1}^{n-1}}{2\Delta x} + \frac{\left(h_i^n\right)^3}{3}\frac{u_{i+1}^{n-1} - 2u_i^{n-1} + u_{i-1}^{n-1}}{\Delta x^2}. \end{aligned} \tag{6}$$

In particular this is an explicit numerical method for (1b), that requires the current and previous values of h and u.

The Lax Wendroff Method for Conservation of Mass Equation

Because the conservation of mass equation (1a) has no mixed derivative term a wider range of numerical methods can be used. This paper will use two, one using the Lax Wendroff method as was done by El et al. (2006) and the other will use the same process as []. Both of these are theoretically second-order accurate. To make these methods precise they will be presented here in sufficient replicable detail.

Note that (1a) is in conservative law form for h where the Jacobian is u. Thus using the previously defined spatio-temporal discretisation the lax-wendroff update for h is

$$\begin{aligned} h_i^{n+1} = & h_i^n - \frac{\Delta t}{2\Delta x}\left((uh)_{i+1}^n - (uh)_{i-1}^n\right) \\ & + \frac{\Delta t^2}{2\Delta x^2}\left(\frac{u_{i+1}^n - u_i^n}{2}\left((uh)_{i+1}^n - (uh)_i^n\right) - \frac{u_i^n - u_{i-1}^n}{2}\left((uh)_i^n - (uh)_{i-1}^n\right)\right). \end{aligned} \tag{7}$$

Preforming this update for all i will be denoted by $\mathcal{E}_h(\boldsymbol{u}^n, \boldsymbol{h}^n, \Delta x, \Delta t)$.

Second Order Finite Difference Method

To follow the process above [] to obtain a second-order finite difference approximation to (1a) the derivatives are first expanded then approximated by second order centered finite differences to give

$$\frac{h_i^{n+1}-h_i^{n-1}}{2\Delta t}+u_i^n\frac{h_{i+1}^n-h_{i-1}^n}{2\Delta x}+h_i^n\frac{u_{i+1}^n-u_{i-1}^n}{2\Delta x}=0. \tag{8}$$

After rearranging this to give an update formula one obtains

$$h_i^{n+1}=h_i^{n-1}-\Delta t\left(u_i^n\frac{h_{i+1}^n-h_{i-1}^n}{\Delta x}+h_i^n\frac{u_{i+1}^n-u_{i-1}^n}{\Delta x}\right). \tag{9}$$

Preforming this update for all i will be denoted by $\mathcal{G}_h\left(\boldsymbol{u}^n,\boldsymbol{h}^n,\boldsymbol{h}^{n-1},\Delta x,\Delta t\right)$.

The Finite Difference Methods

To summarise the first numerical method which naively approximates all derivatives by finite differences has the following update algorithm

$$\left.\begin{aligned}\boldsymbol{h}^{n+1}&=\mathcal{G}_h\left(\boldsymbol{u}^n,\boldsymbol{h}^n,\Delta x,\Delta t\right)\\ \boldsymbol{u}^{n+1}&=\mathcal{G}_u\left(\boldsymbol{u}^n,\boldsymbol{h}^n,\boldsymbol{u}^{n-1},\boldsymbol{h}^{n-1},\Delta x,\Delta t\right)\end{aligned}\right\}\mathcal{G}\left(\boldsymbol{u}^n,\boldsymbol{h}^n,\boldsymbol{u}^{n-1},\boldsymbol{h}^{n-1},\Delta x,\Delta t\right). \tag{10}$$

While the second method which follows from a naive interpretation of the numerical method described by El et al. (2006) is

$$\left.\begin{aligned}\boldsymbol{h}^{n+1}&=\mathcal{E}_h\left(\boldsymbol{u}^n,\boldsymbol{h}^n,\Delta x,\Delta t\right)\\ \boldsymbol{u}^{n+1}&=\mathcal{G}_u\left(\boldsymbol{u}^n,\boldsymbol{h}^n,\boldsymbol{u}^{n-1},\boldsymbol{h}^{n-1},\Delta x,\Delta t\right)\end{aligned}\right\}\mathcal{E}\left(\boldsymbol{u}^n,\boldsymbol{h}^n,\boldsymbol{u}^{n-1},\boldsymbol{h}^{n-1},\Delta x,\Delta t\right). \tag{11}$$

CONSERVATIVE FORM OF THE SERRE EQUATIONS

To overcome the aforementioned difficulty of mixed derivatives the Serre equations (1) can be reformulated into conservative form which has no mixed spatio-temportal derivatives. This is accomplished by the introduction of a new quantity (Le Métayer et al. 2010; Zoppou 2014)

$$G=uh-h^2\frac{\partial h}{\partial x}\frac{\partial u}{\partial x}-\frac{h^3}{3}\frac{\partial^2 u}{\partial x^2}. \tag{12}$$

Consequently, (1) can be rewritten as

$$\frac{\partial h}{\partial t}+\frac{\partial (uh)}{\partial x}=0 \tag{13a}$$

and

$$\frac{\partial G}{\partial t}+\frac{\partial}{\partial x}\left(Gu+\frac{gh^2}{2}-\frac{2h^3}{3}\frac{\partial u}{\partial x}\frac{\partial u}{\partial x}\right)=0. \tag{13b}$$

A Hybrid Finite Difference-Volume Method for Serre Equations in Conservative Form

[] also offer another family of numerical methods which can be constructed by first rearranging the equations into conservative form and then using both a finite difference and a finite volume method to solve these equations. This paper will make use of the first-, second- and third-order versions of this method as set out in []. These have been validated for both smooth and discontinuous problems and their orders of accuracy have been verified for smooth solutions so they are of particular interest for the comparisons that will be investigated in this paper.

NUMERICAL SIMULATIONS

In this section the methods introduced in this paper will be validated by using them to approximate an analytic solution of the Serre equations, this will also be used to verify their order of accuracy. Then an in depth comparison of using these methods for a smooth approximation to the discontinuous dam break problem will be provided to investigate the behaviour of these equations in the presence of discontinuities. This is a problem that so far has only received a proper treatment in (El et al. 2006), with other research giving only a cursory look into the topic.

SOLITON

Currently cnoidal waves are the only family of analytic solutions to the Serre equations (Carter and Cienfuegos 2011). Solitons are a particular instance of cnoidal waves that travel without deformation and have been used to verify the convergence rates of the described methods in this paper.

For the Serre equations the solitons have the following form

$$h(x,t) = a_0 + a_1 \operatorname{sech}^2(\kappa(x - ct)), \tag{14a}$$

$$u(x,t) = c\left(1 - \frac{a_0}{h(x,t)}\right), \tag{14b}$$

$$\kappa = \frac{\sqrt{3a_1}}{2a_0\sqrt{a_0 + a_1}} \tag{14c}$$

and

$$c = \sqrt{g(a_0 + a_1)} \tag{14d}$$

where a_0 and a_1 are input parameters that determine the depth of the quiescent water and the maximum height of the soliton above that respectively. In the simulation $a_0 = 10\text{m}$, $a_1 = 1\text{m}$ for $x \in [-500\text{m}, 1500\text{m}]$ and $t \in [0\text{s}, 100\text{s}]$. With $\Delta t = 0.01\Delta x$ which satisfies [] and $\theta = 1.2$ for the second-order finite difference-volume method.

SMOOTHED DAM-BREAK

The discontinuous dam-break problem can be approximated by a smooth function using the hyperbolic tangent function. Such an approximation will be called a smoothed dam-break problem and will be defined as such

$$h(x,0) = h_0 + \frac{h_1 - h_0}{2}\left(1 + \tanh\left(\alpha\left(x_0 - x\right)\right)\right), \tag{15a}$$

$$u(x,0) = 0.0m/s. \tag{15b}$$

Where a is given and controls the width of the transition between the two dam-break heights of h_0 and h_1. For large α the width is small and vice versa. For a fixed Δx there are large enough α values such that the transition width is zero. This experiment was run for both of the methods described in this paper and the 3 different order finite difference-volume methods described in []. In this particular simulation $h_0 = 1.0m$, $h_1 = 1.8m$ on $x \in [0m, 1000m]$ for $t \in [0s, 30s]$ with $x_0 = 500m$. The simulations were run changing both Δx and α and for stability $\Delta t = 0.01\Delta x$ while for the second-order finite volume method $\theta = 1.2$. Since this experiment involves a very large amount of data the analysis will be broken up into three sections: decreasing Δx, increasing α and finally differences between the methods.

Changing Δx

Decreasing Δx allows the numerical method to better approximate the analytic solution to the equations. So for our valid [] numerical methods it would be expected that smaller Δx's provide a closer approximation to the analytic solution This was demonstrated for smooth problems [] above.

In this comparison we pick an α and a method and investigate the result of decreasing Δx. Because the smoothness of the initial conditions depends on both Δx and α one must be careful that the initial conditions do not change from discontinuous to smooth as Δx is altered as then we are no longer comparing smooth problems. This is of particular importance for the two finite difference methods as they do not correctly handle discontinuos initial conditions. []

The first and most important observation is that there are four types of behaviour as $\Delta x \to 0$ of the problem depending on the α and the numerical method. It was found

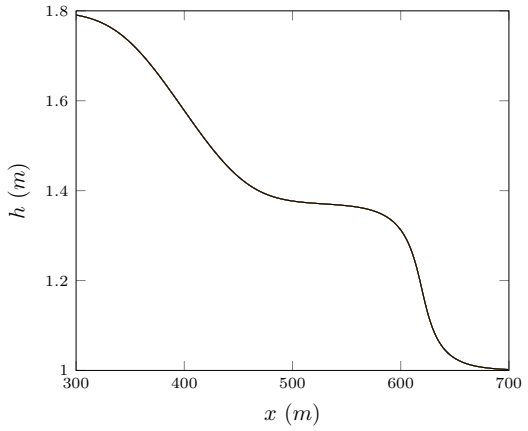

(a)

FIG. 2: Smooth dam break problem for o3 [] with $\alpha = 0.025$ for $\Delta x = 10/2^{10}$ (blue), $\Delta x = 10/2^{9}$ (green), $\Delta x = 10/2^{8}$ (red), $\Delta x = 10/2^{7}$ (cyan), $\Delta x = 10/2^{6}$ (magenta), $\Delta x = 10/2^{5}$ (yellow), $\Delta x = 10/2^{4}$ (black)

that the second- and third-order methods had similar α ranges determining the trending behaviour while the first-order had very different ranges, because of this large difference the term higher-order will be used to refer to all second- and third- order methods. Also for the purposes of simplicity these scenario's will be demonstrated by solutions of the FDVM as they are better for illustrative purposes. The four scenarios are identified by the behaviour of the solutions when Δx is small and they correspond to different results in the literature.

The first behaviour which will be referred to as the non-oscillatory scenario has such smooth initial conditions that there are no introduced oscillations. This scenario ends at $\alpha = 0.025$ and should in theory extend down to the trivial $\alpha = 0$, in these ranges the smoothed dam-break problem is a very poor approximation to the dam-break problem. This behaviour was observed for all methods when $\alpha = 0.025$ and an example case for the third-order method is plotted in Figure 2. This example demonstrates rapid convergence with all the solutions being graphically identical. This scenario resembles the solution of the shallow water wave equations in that it contains only a rarefaction and a shock with no dispersion.

The second will be referred to as the flat scenario due to the presence of a constant height state between the oscillations at the shock and rarefaction fan. This scenario emerges at $\alpha = 0.05$ and continues to $\alpha = 1$ for the higher-order methods and occurs from $\alpha = 0.05$ to $\alpha = 1000$ for the first-order method (so far). This scenario corresponds to the

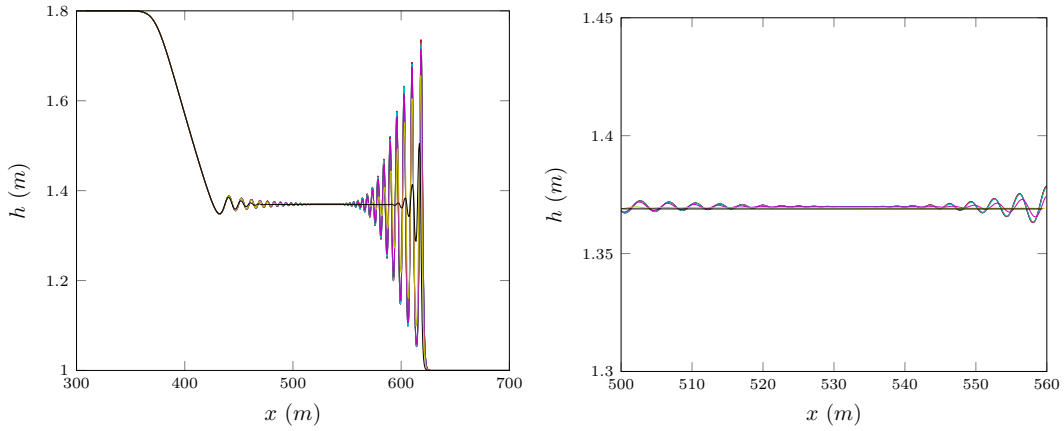

(a) (b)

FIG. 3: Smooth dam break problem for o3 [] with $\alpha = 0.5$ for $\Delta x = 10/2^{10}$ (blue), $\Delta x = 10/2^{9}$ (green), $\Delta x = 10/2^{8}$ (red), $\Delta x = 10/2^{7}$ (cyan), $\Delta x = 10/2^{6}$ (magenta), $\Delta x = 10/2^{7}$ (yellow), $\Delta x = 10/2^{8}$ (black)

results presented by Le Métayer et al. (2010) and Mitsotakis et al. (2014).

An example plot demonstrating this scenario for the third-order method with $\alpha = 0.5$ can be seen in Figure 3. As Δx decreases the solutions converge which is sensible since for the Δx in Figure [] the initial conditions are smooth as can be seen in Figure [] and these methods have been verified for smooth problems. So that by $\Delta x = 10/2^{8}$ the solutions for higher Δx are graphically identical.

The third scenario will be referred to as the contact discontinuity scenario due to the use of that term to describe it by El et al. (2006). For the higher-order methods it occurs at $\alpha = 2.5$ and so far has not occurred for the first order method[]. The contact discontinuity scenarios main feature is that the oscillations from the rarefaction fan and the shock decay and appear to meet at a point as can be seen in Figure 4. For the experiments performed this doesn't appear to be an actual centre point but rather that the oscillations decay so quickly around the 'contact discontinuity' that it appears to be the case. All the higher order methods so far have not shown a converged solution as Δx decreases. However it does appear that convergence is likely with the solutions getting closer together.

The fourth scenario will be referred to as the bump scenario due to the oscillations no longer decaying down towards a point but rather growing around where the contact discontinuity was in the previous scenario as can be seen in Figure 5. This behaviour has hitherto not been presented and is certainly not an expected result. There are some important observations, changing α does increase the height of the bump for the lowest

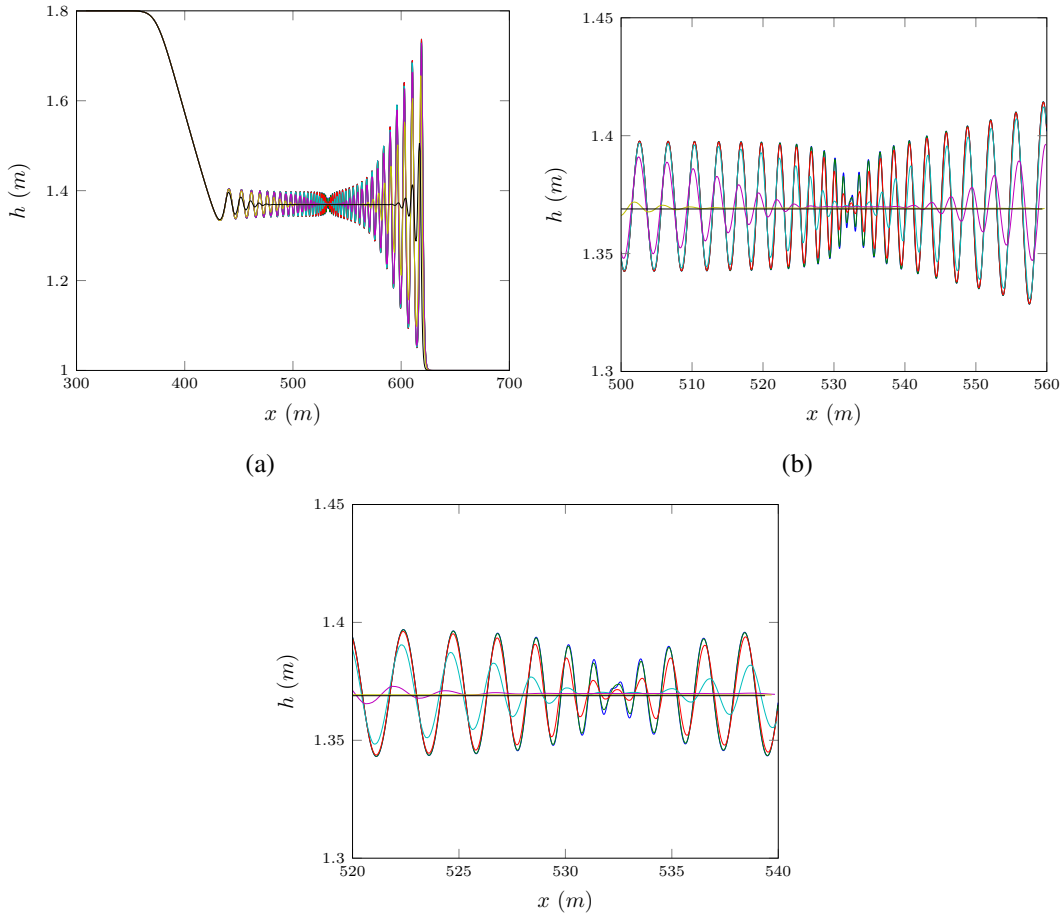

FIG. 4: Smooth dam break problem for o3 [] with $\alpha = 2.5$ for $\Delta x = 10/2^{10}$ (blue), $\Delta x = 10/2^{9}$ (green), $\Delta x = 10/2^{8}$ (red), $\Delta x = 10/2^{7}$ (cyan), $\Delta x = 10/2^{6}$ (magenta), $\Delta x = 10/2^{5}$ (yellow), $\Delta x = 10/2^{4}$ (black)

resolution methods although after [] increasing α has no effect[huh?]. The behaviour of these solutions in Figure 5 do not clearly show convergence, although it doesn't appear that there is a rapid divergence which suggests that this behaviour is not unstable. Also the lack of convergence is only around the contact discontinuity with other parts of the solution showing convergence.

All of the scenarios described above and displayed using the higher-order FDVM also occur for the FDM, however because finite differences cannot properly handle discontinuities this is a little more subtle. Firstly, since for each α there is a Δx such that for larger

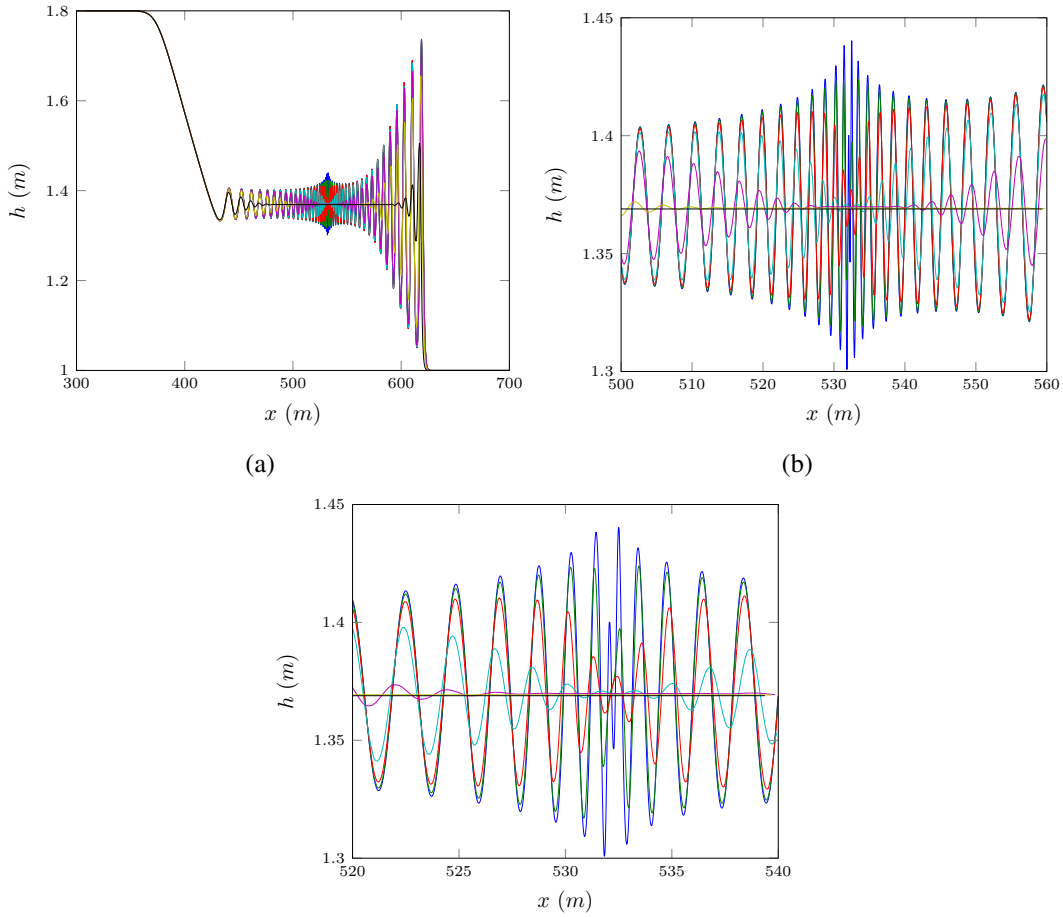

FIG. 5: Smooth dam break problem for o3 [] with $\alpha = 1000.0$ for $\Delta x = 10/2^{10}$ (blue), $\Delta x = 10/2^{9}$ (green), $\Delta x = 10/2^{8}$ (red), $\Delta x = 10/2^{7}$ (cyan), $\Delta x = 10/2^{6}$ (magenta), $\Delta x = 10/2^{7}$ (yellow), $\Delta x = 10/2^{8}$ (black)

Δx the smooth dam break problem is no longer smooth enough for a finite difference approximation to be appropriate. This becomes a problem for the contact discontinuity and bump scenarios since they require higher α and are thus more discontinuous to begin with. The result of this are non-physcial looking oscillations for large Δx values that were not replicated by the FDVM and thus can be attributed to this flaw of FDM as in Figure [].

Overall there where two types of trending behaviours as Δx was decreased one for the FDM and another for the FDVM. FDM decreased the number of oscillations in the solution as in Figure [], while FDVM increased the number of oscillations in the solution as can

be seen in Figure []. This is explained by Zoppou and Roberts (1996) as the FDM are second order finite difference approximations their errors are dissipative thus introducing oscillatory errors which are most prominent when Δx and therefore the errors are large. While the behaviour of the FDVM is explained by a series of effects [] [TVD, treating things as cell averages, thus flattening things in cells,].

[](verify convergence rates near discontinuities?)

Changing α

Increasing α allows the initial conditions (7) to approach the dam break problem with h_1 to the left and h_0 to the right centred around x_0. So it would be expected that as $\alpha \to \infty$ that the solution of the smooth dam break problem would approach the corresponding dam break problem. This is the case for numerical methods because for a fixed Δx α can be chosen large enough that (7) is precisely the dam break problem. This can be seen in Figure [] with Δx = where the required α for this to occur is below 1000 which was the maximum α value used in these experiments. However, only the FDVM were able to handle such large α's because the initial conditions are not smooth enough to allow for stability in the FDM as can be seen in Figure []. While the FDVM handled this quite well and for all Δx tested as α increased the solutions converged, even though for higher Δx [] α was not large enough to make (7) a jump discontinuity.

This confirms the superiority of the FDVM to handle non smooth initial conditions and the inability of FDM to handle them. Even near discontinuous initial conditions caused problems for the FDM with the introduction of oscillations that were not replicated by the FDVM and appeared to be non-physical. An example of these transitional solutions between the properly smooth initial conditions and the unstable discontinuous ones can be seen in Figure []. [](only compare the models when FD started smooth enough)

For the range of α's which are smooth enough for the FDM to be appropriate then as α increases the number of oscillations increases as well for both the FDM and the FDVM. So that the smoothness of the initial conditions controls the oscillations but this depends on Δx since for a fixed α the smoothness of the discretised initial conditions depends on Δx. [] (relative smoothness, more universal number)

It was observed that Δx can be chosen large enough such that increasing α does not resolve some of the more complex structure observed for smaller Δx values. This Δx depends on the model most notably for the first-order finite difference-volume scheme this Δx is very small. An example of this for the third-order FDVM scheme can be seen in Figure [].

Comparison of Models

The first-order FDVM was too diffuse and

CONCLUSIONS

ACKNOWLEDGEMENTS

REFERENCES

Carter, J. D. and Cienfuegos, R. (2011). "Solitary and cnoidal wave solutions of the Serre equations and their stability." *European Journal of Mechanics B/Fluids*, 30(3), 259–268.

El, G., Grimshaw, R. H. J., and Smyth, N. F. (2006). "Unsteady undular bores in fully nonlinear shallow-water theory." *Physics of Fluids*, 18(027104).

Lannes, D. and Bonneton, P. (2009)." *Physics of Fluids*, 21(1), 16601–16610.

Le Métayer, O., Gavrilyuk, S., and Hank, S. (2010). "A numerical scheme for the Green-Naghdi model." *Journal of Computational Physics*, 229(6), 2034–2045.

Li, M., Guyenne, P., Li, F., and Xu, L. (2014). "High order well-balanced CDG-FE methods for shallow water waves by a Green-Naghdi model." *Journal of Computational Physics*, 257, 169–192.

Mitsotakis, D., Dutykh, D., and Carter, J. (2014). "On the nonlinear dynamics of the traveling-wave solutions of the serre equations." *arXiv preprint arXiv:1404.6725*.

Su, C. H. and Gardner, C. S. (1969). "Korteweg-de Vries equation and generalisations. III. Derivation of the Korteweg-de Vries equation and Burgers equation." *Journal of Mathematical Physics*, 10(3), 536–539.

Zoppou, C. (2014). "Numerical solution of the One-dimensional and Cylindrical Serre Equations for Rapidly Varying Free Surface Flows." Ph.D. thesis, Australian National University, Australian National University.

Zoppou, C. and Roberts, S. (1996). "Behaviour of finite difference schemes for advection diffusion equations." *Technical Report Mathematics Research Report No.MRR 062-96*.